

Paleoceanography and Paleoclimatology



RESEARCH ARTICLE

10.1029/2019PA003758

Key Points:

- Latitudinal movement of the ITCZ and South Pacific High
- Shoaling of the East Pacific thermocline
- Closure of the Central American Seaway

Correspondence to:

T. A. Ronge,
thomas.ronge@awi.de

Citation:

Ronge, T. A., Nürnberg, D., & Tiedemann, R. (2020). Plio-Pleistocene variability of the East Pacific thermocline and atmospheric systems. *Paleoceanography and Paleoclimatology*, 35, e2019PA003758. <https://doi.org/10.1029/2019PA003758>

Received 17 AUG 2019

Accepted 8 JAN 2020

Accepted article online 10 JAN 2020

Plio-Pleistocene Variability of the East Pacific Thermocline and Atmospheric Systems

T. A. Ronge¹, D. Nürnberg², and R. Tiedemann¹

¹Alfred-Wegener-Institut Helmholtz-Zentrum für Polar- und Meeresforschung, Bremerhaven, Germany, ²GEOMAR, Helmholtz-Zentrum für Ozeanforschung, Kiel, Germany

Abstract The transition from the Pliocene to the Pleistocene was accompanied by major tectonic reorganizations of key oceanic gateways. In particular, the gradual closure of the Panama Gateway and the constriction of the Indonesian Gateway significantly affected the structure of the Pacific thermocline. In the East Pacific, the thermocline shoaled from an early Pliocene El Niño-like depth to its modern state, which had significant implications for global climate. Here we use Mg/Ca temperature estimates from subsurface and thermocline dwelling foraminifera to reconstruct the meridional Plio-Pleistocene evolution of the Southeast Pacific thermocline, in relation to atmospheric circulation changes. In combination with similar reconstructions from the north-equatorial Pacific, our data indicate a change in the thermocline, responding to the northward displacement of the Intertropical Convergence Zone/South Pacific High system between ~3.8 and 3.5 Ma. After 3.5 Ma, we record a second major phase of thermocline shoaling, which points to the Intertropical Convergence Zone/South Pacific High-system movement toward its modern position along with the gradual cooling of the Northern Hemisphere and its associated glaciation. These findings highlight that a warming globe may affect equatorial regions more intensively due to the potential temperature-driven movement of the Intertropical Convergence Zone/South Pacific High and their associated oceanic systems.

Plain Language Summary Over the course of the last 5 million years (Ma), two oceanic gateways experienced changes due to major tectonic reorganizations. At ~4.4 Ma, the passage connecting the Atlantic and Pacific closed when the connection between the Americas — the Panama land bridge — formed. On the western side of the Pacific, the formation of volcanic islands around Indonesia and Papua New Guinea at ~3.5–3 Ma hampered the transport of tropical water from the Pacific into the Indian Ocean. These processes significantly changed the ocean dynamics and should have altered the tropical Pacific temperature distribution from potential permanent El Niño-like conditions (warm west, warm east) to the modern state. We present sea surface and subsurface temperature reconstructions for the tropical East Pacific off Chile covering the last 5 Ma. Our data imply that the Intertropical Convergence Zone and the South Pacific High moved toward the north along with the warming Northern Hemisphere from ~3.8 to 3.5 Ma. Parallel to the subsequent cooling and glaciation of the Northern Hemisphere, the East Pacific Intertropical Convergence Zone/South Pacific High gradually moved toward their modern position. Ultimately, our data show how hemispherical warming/cooling can affect the position of the Intertropical Convergence Zone/South Pacific High and their associated systems of oceanic temperatures.

1. Introduction

The last 5 million years, spanning the early Pliocene to the late Pleistocene, mark a time period of radical changes in Earth's climate. During this interval, the entire globe evolved from warmer than present conditions toward the cooler icehouse climate of the Pleistocene (Filippelli & Flores, 2009; Haywood et al., 2009; Lisiecki & Raymo, 2007; Raymo et al., 2006). The Pliocene was marked by temperatures ~2 °C to ~3 °C warmer (Haywood et al., 2009), significantly higher CO₂ levels at ~400 ppm — similar to the ~414 ppm reached due to our combustion of fossil fuels (Pagani et al., 2010; Raymo et al., 1996; Seki et al., 2010) — and global sea level 12 to 20 m higher (Miller et al., 2019) than in the preindustrial Holocene period. These factors make the Pliocene a valued (yet not identical) analogue for the predicted future climate change (Bonham et al., 2009; Dowsett & Robinson, 2009; Lunt et al., 2009). Furthermore, some studies indicate that the Pliocene might have experienced permanent El Niño-like conditions in the Pacific Ocean (Bonham et al., 2009; Ravelo et al., 2004; Wara et al., 2005), with an altered Walker

©2020. The Authors.

This is an open access article under the terms of the Creative Commons Attribution-NonCommercial License, which permits use, distribution and reproduction in any medium, provided the original work is properly cited and is not used for commercial purposes.

circulation and — as a result — a deepened thermocline in the tropical East Pacific (TEP; Etourneau et al., 2010; Ravelo et al., 2004; Wara et al., 2005).

Accordingly, a climate warming-related change in El Niño–Southern Oscillation behavior is among the policy-relevant tipping elements (Lenton et al., 2008). Global climate modeling studies have demonstrated that additional anthropogenic forcing may lead to more frequent El Niño events due to reduced temperature gradients in the eastern equatorial Pacific (Cai et al., 2014; Latif et al., 2015; Timmermann et al., 1999).

The notion of permanent El Niño-like conditions, however, is not unchallenged. Coral $\delta^{18}\text{O}$ data from the West Pacific point to Pliocene conditions rather similar to modern El Niño–Southern Oscillation dynamics (Watanabe et al., 2011). Further, the re-evaluation of low-latitude temperature reconstructions arguing for permanent El Niño-like conditions (e.g., Wara et al., 2005) showed that the Western Pacific Warm Pool and the eastern cold tongue might have maintained their zonal temperature gradient throughout the Pliocene (Zhang et al., 2014). Notably, during the Mid-Pliocene (~4.5–3 Ma) tectonic changes of important oceanic gateways are considered to have significantly reorganized the deep thermohaline circulation, ultimately resulting in the transition to the colder Pleistocene climate. The closure of the Central American Seaway (CAS; Panama) has experienced its most critical phase just during this time interval (Haug et al., 2001; Haug & Tiedemann, 1998). The constriction and final closure of the CAS led to the intensification of both the Gulf Stream and, in a broader perspective, the Atlantic Meridional Overturning Circulation, leading to commonly higher sea surface temperatures (SSTs; Haug & Tiedemann, 1998; Haug et al., 2001; Karas et al., 2017) and salinities (Keigwin, 1982) in the Caribbean sector of the western Atlantic. At the same time, the East Pacific experienced a decline in surface temperatures, the intensification of costal upwelling (Dekens et al., 2007; Ibaraki, 1997), and the shoaling of the tropical East Pacific thermocline (Steph et al., 2006). Ultimately, the closure of the CAS is thought to have preconditioned the initiation of the Northern Hemisphere glaciation (NHG; Haug & Tiedemann, 1998; Haug et al., 2001; Karas et al., 2017; Lunt et al., 2007). The Indonesian Gateway is also considered as a major driver of the reorganization of the Plio-Pleistocene oceanic and climatic system (Cane & Molnar, 2001; Karas et al., 2009). The constriction of this gateway, in particular between 3.5 and 2.95 Ma, intensified the West Pacific Warm Pool, deepened the tropical Indian Ocean thermocline, and thereby fostered the formation of the East Pacific cold tongue (Karas et al., 2009, 2017).

By providing new Mg/Ca-derived temperature records from surface to deep-dwelling planktic foraminiferal species from ODP Site 1236 (~1,100 km off northern Chile), we further constrain the spatiotemporal evolution of the tropical East Pacific thermocline as well as new insight into the position of the Intertropical Convergence Zone (ITCZ) and the South Pacific High (SPH). The location of Site 1236 is ideal in this respect, for further constraining the shoaling and finally the closure of the CAS.

1.1. Regional Oceanography

Despite the fact that throughout the last 5 Ma the eastward drift of the Nazca Plate moved the location of Site 1236 about 185 km closer toward the South American continent (Meschede & Barckhausen, 2000), it is considered that oceanic and sedimentary parameters remained similar to modern conditions over this time period (Mix et al., 2003b).

Propelled by the perpetual force of the Southeast trade winds, deep waters shoal along the Peruvian coast (Kessler, 2006; Strub et al., 1998). Associated with the position of the ITCZ, moving toward the north during the austral winter (Strub et al., 1998), the upwelling intensity increases (Karstensen & Ulloa, 2008; Letelier et al., 2009), likewise decreasing SSTs in the TEP (Cane, 2005). Similar to the north-south movement of the ITCZ, the position of the SPH as well is driven by a seasonal migration toward the warmer hemisphere (Schneider et al., 2017). However, due to its remote position, the costal upwelling does not directly influence Site 1236; thus, it is recording more oligotrophic subtropical gyre conditions (Mix et al., 2003b).

Subtropical Surface Water (SSW) is characterizing the surface parameters in our research area ~21° south of the equator with SSTs around 20 °C and a salinity of more than 35‰ (Strub et al., 1998). The SSW is formed by increased evaporation rates in this area (Strub et al., 1998). To the east, the mixing of SSW and cold upwelled water results in Cold Coastal Water, colder than ~19 °C, which is dominating the surface waters up to the South American Coast (Ayón et al., 2008). North of the area occupied by SSW, mixing of SSW, Cold Coastal Water, and North Pacific Tropical Surface Water forms Equatorial Surface Water (Strub et al.,

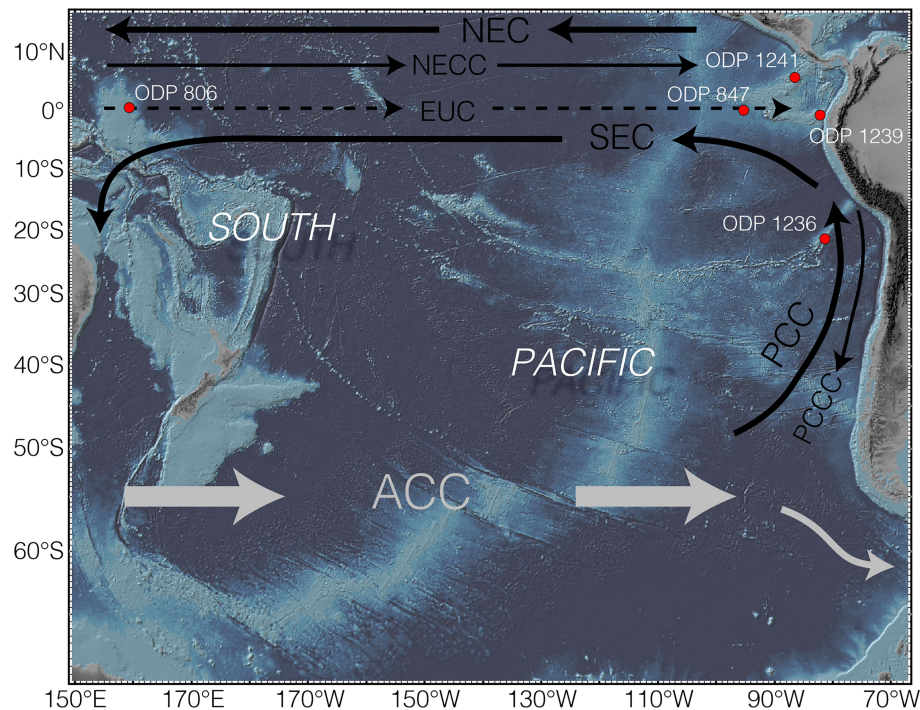


Figure 1. General Pacific circulation patterns (Ayón et al., 2008; Fiedler & Talley, 2006; Mix et al., 2003a). ACC - Antarctic Circumpolar Current, EUC - Equatorial Undercurrent, NEC/SEC - North/South Equatorial Current, NECC - North Equatorial Counter Current, PCC - Peru Chile Current, PCCC - Peru Chile Counter Current. Core locations indicated by red dots. Map created with GeoMapApp.

1998). At the location of Site 1236, South Pacific Eastern Subtropical Mode Water (SPESTMW) is occupying the depth between ~100 and 150 m right underneath SSW (Wong & Johnson, 2003). SPESTMW is defined by its potential vorticity Q smaller than $3 \times 10^{-10} \text{ m}^{-1} \text{ s}^{-1}$ (Wong & Johnson, 2003) and a temperature range of 13–20 °C (Fiedler & Talley, 2006). Further below, Southern Ocean Intermediate Waters (SOIW), comprising of Subantarctic Mode Water and Antarctic Intermediate Water, ventilates the water depth between about 200 and 1,400 m (Fiedler & Talley, 2006; Pena et al., 2013; Rippert et al., 2017).

Located at the Nazca Ridge, Site 1236 is close to the western edge of the northward flowing Peru Chile Current (PCC; Figure 1), one of the globe's four major eastern boundary currents (Strub et al., 1998). The PCC is part of a larger East Pacific current system, sometimes referred to as the Humboldt or Peru Chile Current System. Besides the PCC, the current system includes the poleward directed Peru Chile Counter Current and the Peru Chile Undercurrent (Ayón et al., 2008; Strub et al., 1998). As part of the Subtropical Gyre, the PCC is a conduit for cold, nutrient-rich Subantarctic surface waters toward the equator (Silva et al., 2009). Opposed to that, the Peru Chile Counter Current and the Peru Chile Undercurrent transport warmer equatorial and subtropical surface and subsurface waters toward the south (Silva et al., 2009).

1.2. El Niño–Southern Oscillation and Thermocline Depth

Usually, a temperature gradient prevails between a West Pacific warm pool and cold, nutrient-rich waters in the East Pacific (Figures 2a and 2b). This pattern is accompanied by a deep thermocline off Indonesia and a shallow thermocline off Chile and Peru (Figures 2c and 2d). Typically, every two to seven years, the temperatures in the East Pacific alternate between unusual warm (El Niño) and cold (La Niña) conditions (e.g., McPhaden et al., 2006). Throughout an El Niño event, the equatorial trade winds weaken, resulting in a weakening of the Humboldt Current System and ultimately in reduced upwelling off South America (McPhaden et al., 2006). The decrease in wind stress allows for an eastward flow of warm equatorial waters, relaxing the inclined Pacific thermocline, hence leading to a deepening of the thermocline in the East Pacific (Philander & Fedorov, 2003a; Sun et al., 2004). During so-called La Niña events, stronger winds amplify the “normal” pattern, accumulating warmth in the West Pacific and decreasing thermocline depth in the east (Philander & Fedorov, 2003a; Sun et al., 2004). While not undisputed (Watanabe et al., 2011), several

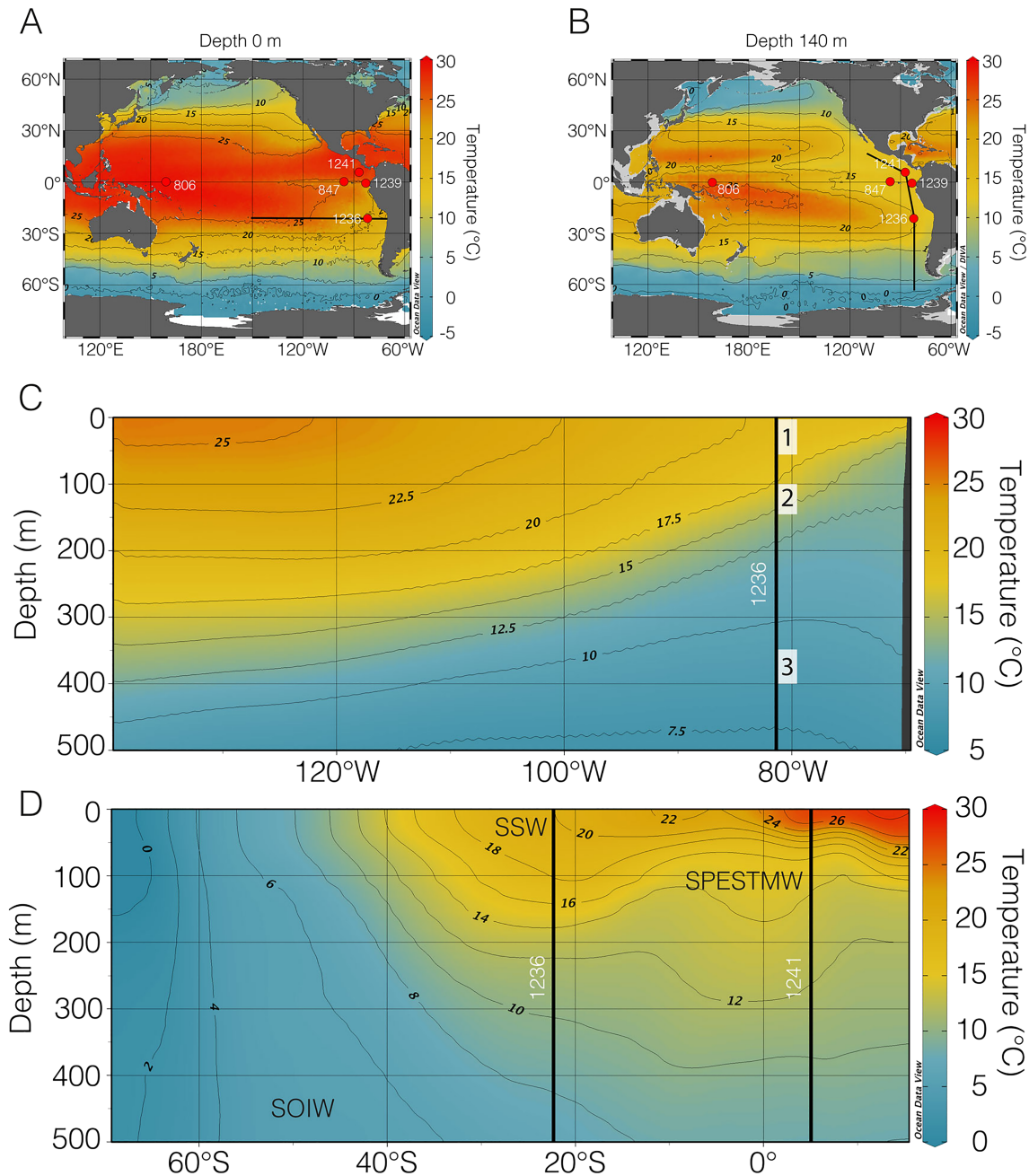


Figure 2. Pacific temperature pattern (Locarnini et al., 2013). (a) Sea surface temperatures. (b) Temperatures at 140-m water depth. (c) Depth section of temperature along the black line indicated in (a). Apparent calcification depth of *T. sacculifer* - 1, *G. tumida* - 2, *G. inflata* - 3. (d) Depth section of temperature along the black line indicated in (b). SSW - Subtropical Surface Water, SOIW - Southern Ocean Intermediate Water, SPESTMW - South Pacific Eastern Subtropical Mode Water. Core locations discussed here are indicated by red dots in (a) and (b) and vertical black lines in (c) and (d). Figure generated using ODV (Schlitzer, 2019). Color palette - Life Aquatic by P. Rafter.

studies have suggested that permanent El Niño-like conditions, with a deep TEP thermocline, prevailed throughout the warmer than present Pliocene between ~5 and 3 Ma (e.g., Fedorov et al., 2006; Philander & Fedorov, 2003b; Steph et al., 2010; Wara et al., 2005).

2. Material and Methods

Our study is based on new data from the tropical East Pacific ODP Site 1236 (Leg 202; 21°21.538'S, 81°26.164' W; Mix et al., 2003a), drilled in a water depth of 1,322 m. All reconstructions follow the mean composite

depth scale of Site 1236 (Mix et al., 2003b). The combination of succeeding and complete sediment sequences from different holes, which forms the mean composite depth record, is given in the data set archived at www.PANGAEA.de, supplementing this manuscript. Sediment samples were freeze-dried and wet-sieved using a 63- μm sieve. Dry samples were split into <125-, 125–250-, 250–315-, 315–400-, and >400- μm size fractions.

2.1. Foraminiferal Species

To reconstruct the temporal and vertical evolution of East Pacific surface to subsurface properties, we analyzed Mg/Ca ratios as well as the stable isotope composition of three different planktic foraminiferal species (*Trilobatus sacculifer* (Spezzaferri et al., 2015) without saclike final chamber, *Globorotalia tumida*, and *Globorotalia inflata*), which are known to occupy different habitat depths within the upper ocean. The habitat occupied by these species relies on different oceanic parameters such as nutrients, light levels, and temperature or the concentration of chlorophyll (Curry et al., 1983; Fairbanks et al., 1980; Fairbanks & Wiebe, 1980; Steph et al., 2006; Watkins et al., 1998).

The symbiont-bearing *T. sacculifer* is known to calcify within the well-lit, nutrient-depleted warm mixed layer (~50 m), down to the upper thermocline (Anand et al., 2003; Curry et al., 1983; Fairbanks et al., 1982; Hemleben et al., 1988; Jentzen et al., 2018; Lynch-Stieglitz et al., 2015; Rippert et al., 2016). Nevertheless, at least some specimens calcify within in deeper waters down to about ~100 m and might therefore record higher $\delta^{18}\text{O}$ values (Duplessy et al., 1981; Lohmann, 1995; Lynch-Stieglitz et al., 2015; Spero et al., 2003). Further down the water column, *G. tumida* is known to live toward the bottom of the photic zone (BOPZ) between ~100 and ~140 m (Lynch-Stieglitz et al., 2015; Ravelo & Fairbanks, 1992; Ravelo & Shackleton, 1995). This habitat depth is close to constant in tropical waters (Steph et al., 2006), making the isotopic composition and Mg/Ca ratios of *G. tumida* ideal to record changes in the depth of the thermocline (today ~100–150 m; Locarnini et al., 2013), as the temperature at the tropical BOPZ is to some extent regulated by the vertical position of the thermocline (Steph et al., 2006). The deep-dwelling *G. inflata* is known to calcify in a broader depth range than the other two species (mixed layer down to >500 m; Groeneveld & Chiessi, 2011). Based on a core-top study from the tropical South Atlantic, the apparent calcification depth (ACD) for the *G. inflata* specimens used by us is reported to range between 350 and 400 m (Groeneveld & Chiessi, 2011). For each species, we selected ~35 well-preserved specimens from the narrow 315–400- μm size fraction (e.g., Steph et al., 2006; Wara et al., 2005). To account for the broader calcification depth of *G. inflata*, we followed the suggestions of Groeneveld and Chiessi (2011) according to which only specimens without a shiny calcite crust and three chambers in the final whorl were selected.

2.2. Mg/Ca Temperatures

For sample treatment, we followed the cleaning procedure of Schmidt and Lynch-Stieglitz (2011), supplemented by a final reductive cleaning step described in Reißig et al. (2019). All samples were measured at the GEOMAR, using a Varian 720-ES ICP OES. The Mg/Ca data were related to the ECRM752-1 standard (Greaves et al., 2008), with a Mg/Ca reference value of 3.762 mmol/mol. Results were further drift corrected, using the ECRM752-1 as internal consistency standard. The long-term precision was ± 0.1 mmol mol⁻¹.

We used the calibration of Anand et al. (2003) for the conversion of both *T. sacculifer* (subsurface temperatures = subSST_{*T. sacculifer*}) and *G. tumida* (thermocline temperatures = TT_{*G. tumida*}) Mg/Ca ratios to temperatures (Mg/Ca = $0.38\exp(0.09 \times T \text{ } ^\circ\text{C})$). For *G. inflata* (deep thermocline temperatures = DTT_{*G. inflata*}), we applied the calibration of Groeneveld and Chiessi (2011) (Mg/Ca = $0.72\exp(0.076 \times T \text{ } ^\circ\text{C})$). These equations were also used by Steph et al. (2006, 2010) and thus allow for a robust comparison of the East Pacific ODP site records. We are aware that the species used by us might have a different sensitivity to calcite dissolution and diagenetic affect. With a water depth of 1,322 m, Site 1236 is situated in slightly calcite unsaturated waters, below the threshold of $\Delta[\text{CO}_3^{2-}]$ of 21.3 $\mu\text{mol kg}^{-1}$ (Regenberg et al., 2014), indicating that Mg²⁺ removal might be of minor concern. However, Site 1236 sits well above the lysocline and carbonate preservation for the time interval covered by this study is excellent (Mix et al., 2003b). Thus, we consider a potential error introduced by dissolution of minor concern. Nonetheless, preferential removal of Mg²⁺ ions might affect absolute temperature reconstructions, but the vertical gradient of our reconstructions and the comparison to similar records remains robust and thus allows for a comparison of subSST, TT, and DTT throughout the record.

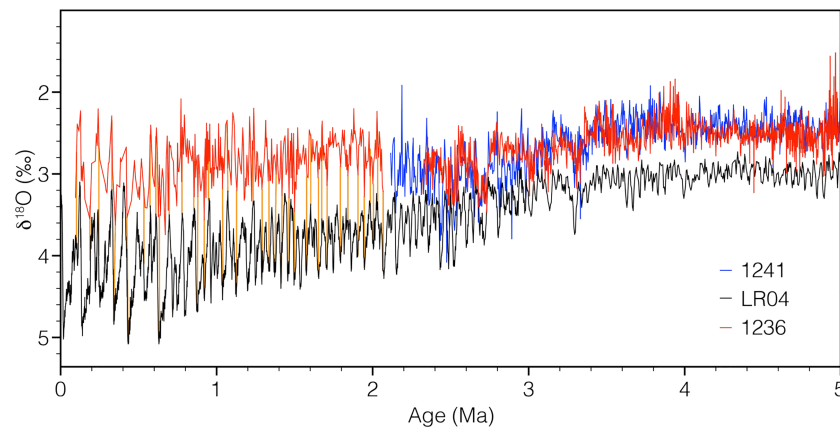


Figure 3. Benthic $\delta^{18}\text{O}$ records of Site 1236 (red; this study; 2.4–5 Ma; Tiedemann et al., 2007), Site 1241 (blue; Tiedemann et al., 2007), and the global benthic stack LR04 (black; Lisiecki & Raymo, 2005). Vertical orange lines indicate the tie lines between Site 1236 (~0 to 2 Ma) and the LR04 Stack.

2.3. Benthic Stable Isotopes

Benthic $^{18}\text{O}/^{16}\text{O}$ isotope ratios (reported in δ notation versus VPDB; calibrated via NBS19 standard) were measured at the Alfred-Wegener-Institute (Bremerhaven, Germany) on *Cibicidoides wuellerstorfi* and *Cibicidoides kullenbergi*, using a Thermo Scientific MAT 253 mass spectrometer coupled to a Kiel IV Carbonate Device. Based on an internal laboratory standard (Solnhofen limestone) the one-year long-term precision was better than $\pm 0.08\text{‰}$. The sampling interval was 2 cm on average. However, we were not able to find at least three monospecific specimens in the interval between ~8 and 9.40 m (~2–2.3 Ma).

2.4. Age Model

For the time interval between ~2.5 and 5 Ma, the initial age model for Site 1236 was established on magnetostratigraphy (Tiedemann et al., 2007). Based on this initial model, benthic $\delta^{13}\text{C}$ and $\delta^{18}\text{O}$ records were visually correlated to the records of orbital-tuned Site 1241 (Tiedemann et al., 2007). In order to extend the age model toward the top of the sediment record (0- to ~8-m composite depth), we correlated the benthic $\delta^{18}\text{O}$ isotope record to the benthic isotope stack LR04 (Lisiecki & Raymo, 2005) using AnalySeries 2.0.4.2 (Paillard et al., 1996). The correlation and tie lines of the Site 1236 isotope record (this study; Tiedemann et al., 2007) to reference Site 1241 and the LR04 stack are displayed in Figure 3 and show a good correlation between both records. Due to the use of these independent methods (magnetostratigraphy, $\delta^{13}\text{C}$, $\delta^{18}\text{O}$, orbital tuning (1241)) we have a high confidence in the age model of Site 1236, in particular for the main interval (2–5 Ma) primarily discussed in this study.

3. Results

3.1. Mg/Ca Temperatures

Over the last 5 million years Mg/Ca ratios varied between 2.19 and 4.04 mmol mol^{-1} for *T. sacculifer*, showing consistently higher Mg/Ca ratios than the other species. For *G. tumida*, Mg/Ca ratios range between 1.29 and 2.36 mmol mol^{-1} and are close for those of *G. inflata* (1.64 and 2.39 mmol mol^{-1} ; Figure 4). According to the ACD of the different planktic foraminiferal species outlined above, the Mg/Ca ratios as well depict a consistent depth distribution with *T. sacculifer* representing subsea surface (subSST), *G. tumida* thermocline (TT), and *G. inflata* deep thermocline (DTT) temperatures throughout the record. Our interpretations assume that the foraminiferal species did not significantly change their habitat depth and apparent calcification depth over the time period covered in this paper.

Small changes (~3.5 °C) in subSSTs are observed throughout the entire record with an average temperature of about 21 °C, close to the modern SST of ~20 °C, as inferred from WOA13 (Locarnini et al., 2013). After about 3.8 Ma (coinciding with the closure of the CAS), temperatures gradually increase by ~1 °C. The most significant deviation from the 5-million-year average, reaching ~27 °C, is recorded between ~2.4 and 2.2 Ma (Figure 4).

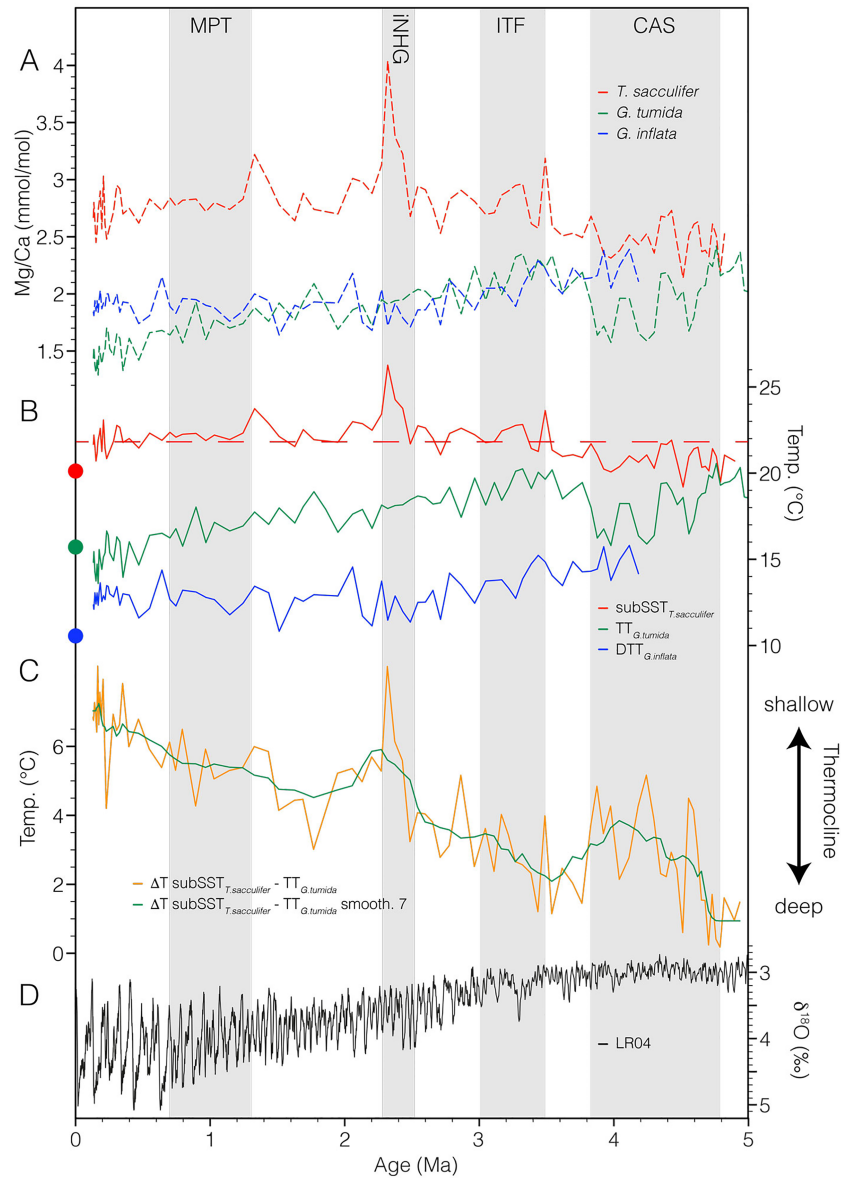


Figure 4. Site 1236 downcore records. (a) Mg/Ca records of *T. sacculifer* (broken red), *G. tumida* (broken green), and *G. inflata* (broken blue). (b) Mg/Ca-based temperatures of *T. sacculifer* — $\text{subSST}_{T. sacculifer}$, *G. tumida* - $\text{TT}_{G. tumida}$, and *G. inflata* - $\text{DTT}_{G. inflata}$. Colored dots indicate modern temperatures at Site 1236 (Locarnini et al., 2013). Red broken line - average $\text{subSST}_{T. sacculifer}$. (c) $\text{subSST}_{T. sacculifer}$ to $\text{TT}_{G. tumida}$ difference (ΔT ; orange), seven-point smoothed ΔT record (green). (d) Global benthic $\delta^{18}\text{O}$ stack (Lisiecki & Raymo, 2005). CAS - intensification of Central American Seaway closure, ITF - intensification of the constriction of the Indonesian Throughflow, iNHG - intensification of Northern Hemisphere Glaciation, MPT - Mid-Pleistocene Transition.

On average, $\text{TT}_{G. tumida}$ are lower than $\text{subSST}_{T. sacculifer}$ (Figure 4). Before ~4.8 Ma however, $\text{TT}_{G. tumida}$ and $\text{subSST}_{T. sacculifer}$ are in a similar range. Between ~4.8 and ~3.8 Ma $\text{TT}_{G. tumida}$ gradually decrease from about 20 °C to 16 °C, parallel to the closure of the CAS. From 3.8 to 3.5 Ma, $\text{TT}_{G. tumida}$ rapidly increase by about 5 °C, almost reaching $\text{subSST}_{T. sacculifer}$ values that also increase by ~1 °C (Figure 4). Following this warming event, $\text{TT}_{G. tumida}$ progressively decrease toward modern values, showing a more dynamic evolution with higher amplitudes than $\text{subSST}_{T. sacculifer}$ values.

The $\text{DTT}_{G. inflata}$ also shows lower amplitudes than $\text{TT}_{G. tumida}$ with a 5-million-year average of about 13 °C, indicating that the BOPZ depth is the most dynamic depth in our study area. While $\text{TT}_{G. tumida}$ rapidly increase, $\text{DTT}_{G. inflata}$ begin to decrease after ~3.8 Ma from 15 °C to 11 °C (Figure 4). For the rest of the $\text{DTT}_{G. inflata}$ record, values oscillate between ~11 °C and ~14 °C but show no visible trend on average.

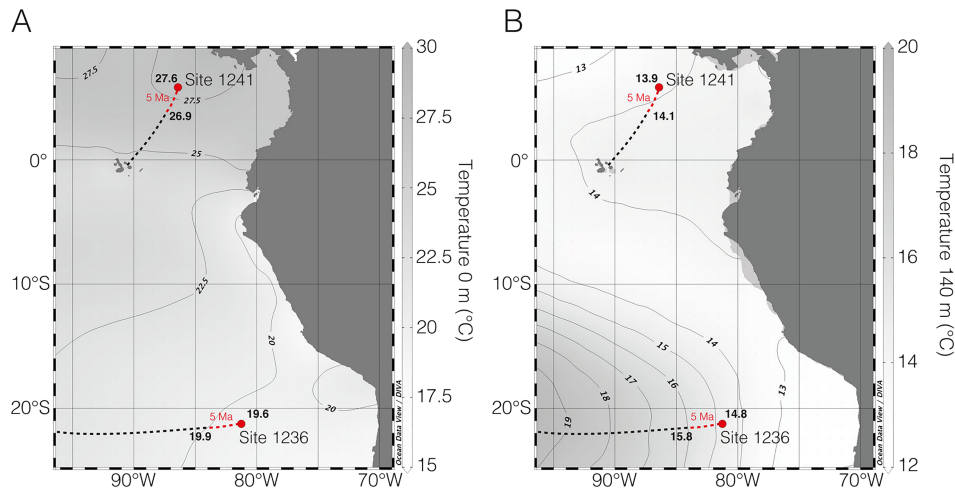


Figure 5. Tectonic backtrack of Sites 1236 and 1241. (a) Sea surface temperatures. (b) Temperatures at the bottom of the photic zone (140 m). Red interval indicates the last 5 Ma. Background grey scale indicates modern temperatures (Locarnini et al., 2013) with bold numbers indicating temperatures at the modern location and the site 5 Ma ago.

The vertical temperature gradient (primarily defined by the subSST_{*T. sacculifer*} and TT_{*G. tumida*} records) progressively increases throughout the record from ~0 °C to ~7 °C (Figure 4). This trend is interrupted by an event between 3.8 and 3.5 Ma, caused by warming TT_{*G. tumida*} and a second event between ~2.3 and ~1.7 Ma, as a result of rapidly warming subSST_{*T. sacculifer*}.

4. Discussion

As we show in Figure 2c, the isotherms steeply slope toward the South American continent. To assess whether or not the observed temperature patterns in our records were caused by changes in oceanic parameters or by the tectonic drift along the backtrack of the sites, we analyzed the temperature distribution along their path. Moving Site 1236 along its backtrack results in no substantial change of subSSTs, TTs, or DTTs (Figure 5). Likewise, we discard the tectonic movement of Site 1241 (Steph et al., 2006) as the potential driver of the temperature pattern between Sites 1236 and 1241. During the time interval in question (~2.6–4 Ma; Figure 6), all changes are driven by the pattern of Site 1236 and not by 1241 temperatures. In our research area, instead, the TT might have been sensitive to a shift in the geographical position of Site 1236 (Figure 5). Nevertheless, this ~3° longitudinal shift might only have accounted for a TT change of 0.7 to 1 °C, a small fraction of the total ~7 °C decrease. Hence, we discard the tectonic effect on the observed temperature patterns and interpret these as changes in the water mass structure of the TEP.

4.1. Plio-Pleistocene Zonal Temperatures

On its own, the East Pacific Site 1236 subSST_{*T. sacculifer*} record (Figure 4) displays no significant feature over the last 5 Ma. The comparison of Site 1236 subSST_{*T. sacculifer*} to the western Pacific record from ODP Site 806 (Wara et al., 2005) shows that Site 1236 temperatures constantly remained below Site 806 values, only interrupted by a warm spike at Site 1236 between ~2.4 and ~2.2 Ma, parallel to the intensification of the NHG (Figure 6). During this brief time interval subSST across the tropical Pacific converge (Figures 6a–6c; Raddatz et al., 2017; Wara et al., 2005), before the modern east-west gradient is fully established. Between ~2.1 and 2.4 Ma, the southwest migration of the South Pacific Convergence Zone (Raddatz et al., 2017) triggered a displacement of the West Pacific Warm Pool, thus reorganizing the temperature patterns across the tropical Pacific. If the additional information from ODP Site 847 (Wara et al., 2005) is considered, the Site 1236 pattern points to permanent El Niño-like conditions between ~3 and 5 Ma. During modern non-El Niño conditions a strong east to west temperature gradient is observed within the Pacific subSST_{*T. sacculifer*}. Propelled by the perpetual motion of the equatorial trade winds, cold deep water shoals along the coast off South America, resulting in a shallow thermocline and colder subSST_{*T. sacculifer*} in the southeast Pacific. During an El Niño event, the trade winds weaken significantly. This mitigation results in the relaxation of

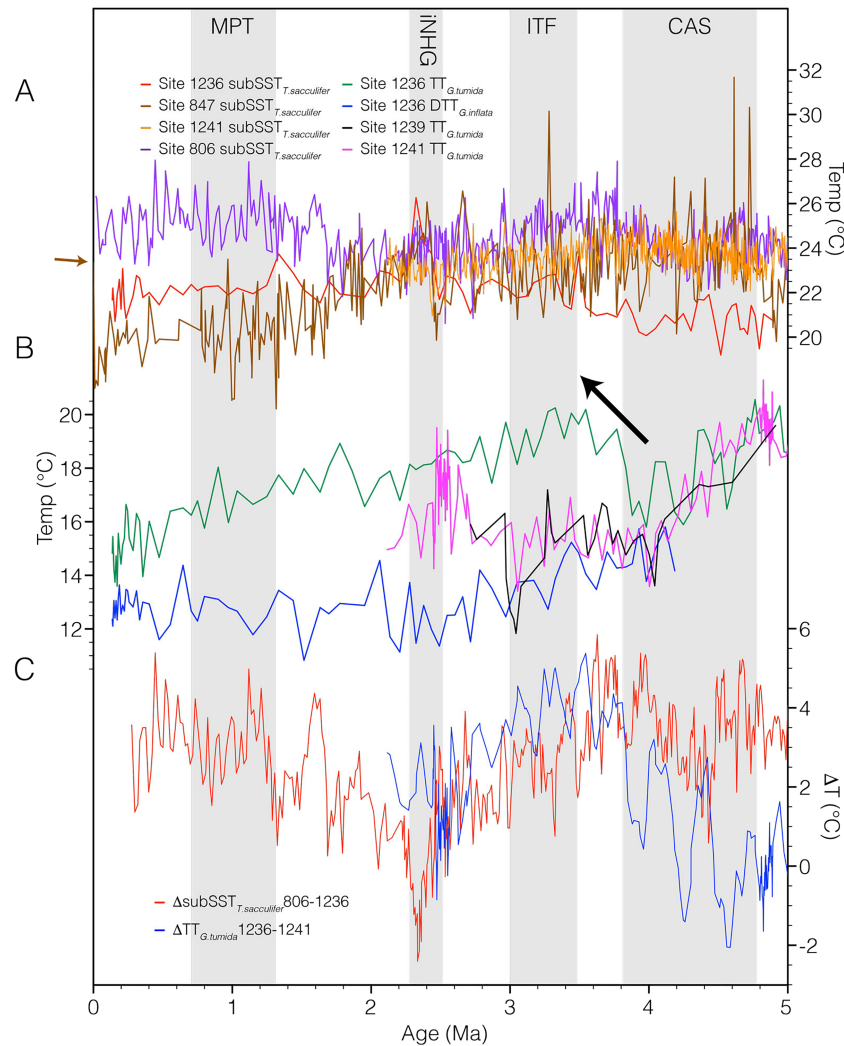


Figure 6. Plio-Pleistocene evolution of East Pacific temperatures. (a) Surface temperatures of Sites 1236 (this study), 847/806 (Wara et al., 2005), and 1241 (Steph et al., 2006). (b) Subsurface temperatures of Sites 1236 (this study), 1239 (Steph et al., 2010), and 1241 (Steph et al., 2006). (c) Temperature gradient of subSST_{*T. sacculifer*} (red) and TT_{*G. tumida*} (blue). The black arrow indicates the northward displacement of the ITCZ/SPH. The brown arrow points to the last data point of Site 847.

the eastward sloping thermocline depth (TCD) and increased subSST_{*T. sacculifer*} in the East Pacific (Cane, 2005; Sun et al., 2004). After ~2.3 Ma the West Pacific subSST_{*T. sacculifer*} start to increase (ODP Site 806; Wara et al., 2005), while the East Pacific temperatures decrease (Site 847; Wara et al., 2005) and/or remain the same (Site 1236; this study). Several studies have attributed this change to the end of the permanent El Niño-like state (e.g., Fedorov et al., 2006; Wara et al., 2005) and the transition toward modern conditions (Figure 6). However, as stated in our introduction, the notion of permanent El Niño-like conditions is not unchallenged and the scientific discussion is far from being settled (Watanabe et al., 2011).

4.2. East Pacific Subsurface to Thermocline Temperatures

Below the surface, an increasing temperature gradient between surface and deeper waters indicates that this transition began almost 2.3 million years before it became apparent in surface temperatures of equatorial Site 847 (Wara et al., 2005) at about 2.4 Ma. We interpret the large increase in the temperature gradient between subsurface waters (*T. sacculifer*), the BOPZ (*G. tumida*), and the deeper waters (*G. inflata*) as the progressive decrease in the depth of the East Pacific thermocline (Figure 7). At Site 1236, the thermocline

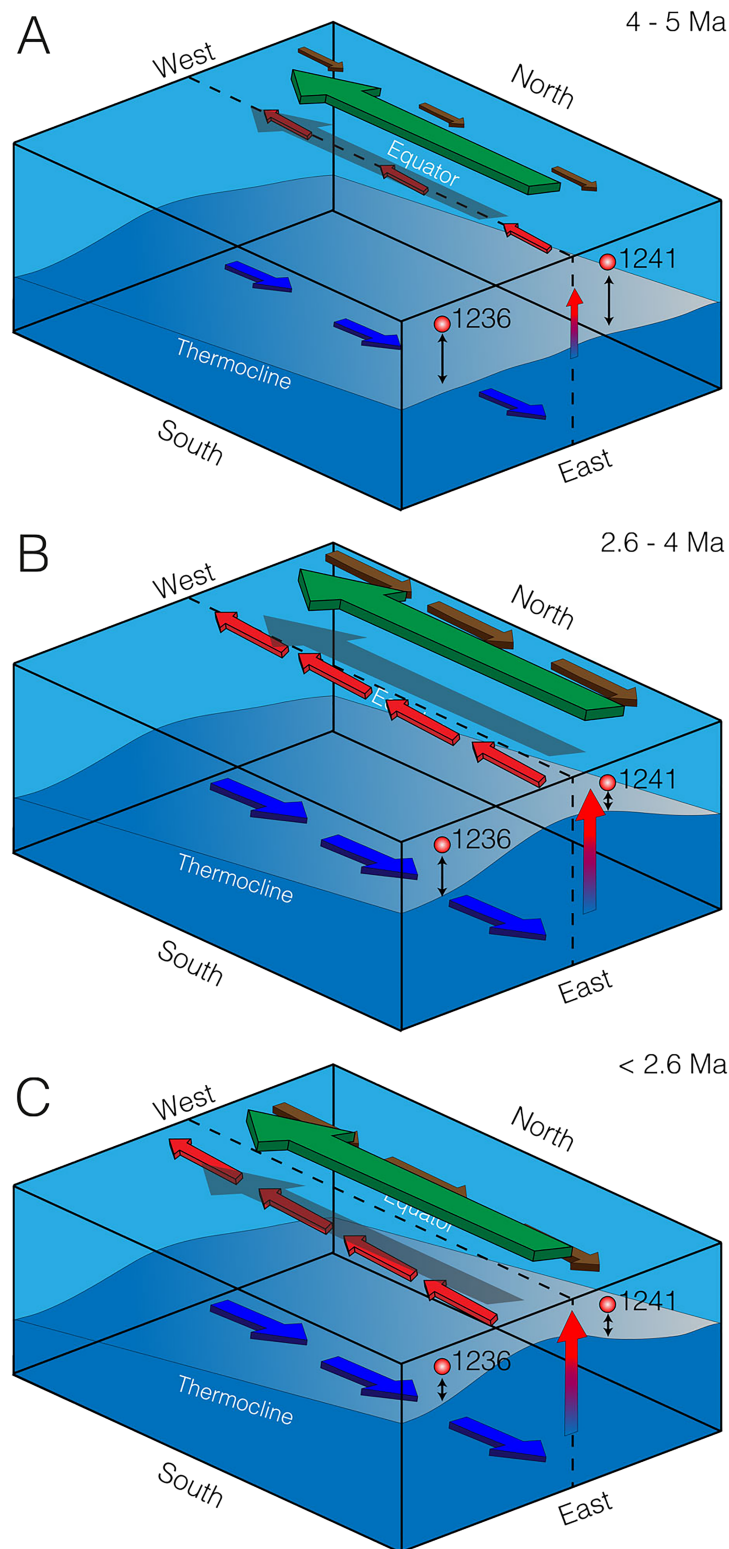


Figure 7. Plio-Pleistocene evolution of East Pacific thermocline structure. (a) Early Pliocene. Tropical Pacific thermocline begins to tilt slightly. BOPZ waters of Site 1236 and Site 1241 experience elevated temperatures. (b) Late Pliocene. Intensification of the westward directed trade winds intensifies upwelling, triggering the shoaling of the thermocline. ITCZ/SPH and associated wind and current systems displaced to the north. BOPZ waters at Site 1241 colder than at Site 1236. (c) Pleistocene. Southward movement of the ITCZ/SPH and associated wind and current systems. Thermocline bulge moves toward the south, relaxation of the temperature gradient between Sites 1236 and 1241; shoaling of thermocline at Site 1236, deepening at Site 1241. Blue arrows - Equatorial Undercurrent, red arrows - South Equatorial Current, blue to red arrow - upwelling, brown arrows - North Equatorial Countercurrent, green arrow - Walker Cell.

was relatively deep during the Early Pliocene from ~5 to 4.5 Ma. During this time, parallel to the closure of the CAS, a gradual cooling of the $TT_{G. tumida}$ marks the first step of thermocline shoaling and is completed at about 4 Ma. This early modification in East Pacific TCD is also observed in the tropical Northeast Pacific record at ODP Site 1241 (Steph et al., 2006) as well as the equatorial ODP Site 1239 (Figures 6 and 7a; Steph et al., 2010). With respect to our reconstructed $subSST_{T. sacculifer}$ temperatures, it is noteworthy that South Pacific $subSST$ were significantly warmer than equatorial temperatures at Site 847 (Figure 6; Wara et al., 2005). The modern East Pacific temperature gradient (Locarnini et al., 2013) indicates a $subSST$ temperature difference of up to 2.5 °C for the calcification depth of *T. sacculifer*, with lower temperatures prevailing at Site 847. We assume that the continuous shoaling of the East Pacific thermocline place Site 847 under the influence of colder waters after ~1.6 Ma.

An interval of warming $TT_{G. tumida}$ and to a lesser extent $subSST_{T. sacculifer}$ temperatures interrupted the transition to colder modern-like conditions at Site 1236, between ~3.8 and 3.5 Ma (Figures 6 and 7b). No such pattern was registered in the deeper $DTT_{G. inflata}$ record. Hence, we assume that the temperature rise reflects a deepening of TCD to a depth between the habitats of *G. tumida* and *G. inflata*. Similar to the modern East Pacific, the subsurface temperatures at all northerly sites are clearly higher than $subSST_{T. sacculifer}$ at Site 1236, during this interval. This pattern is reversed at the habitat depth of *G. tumida*, as the time period between ~3.8 and 2.6 Ma is characterized by $TT_{G. tumida}$, which were up to 5 °C warmer at the southerly Site 1236, compared to the northern Sites 1239 and 1241 (Figure 6; Steph et al., 2006, 2010).

Several mechanisms might be responsible for this observed $TT_{G. tumida}$ warming at Site 1236 (Figure 6): (1) shifting boundaries between SPESTMW and underlying SOIW; (2) rivaling influence of SOIW and North Pacific Intermediate Water (NPIW); or (3) latitudinal shifting of the ITCZ, the SPH, and associated upwelling systems.

As SOIW is significantly colder than overlying SPESTMW (Locarnini et al., 2013), a reduced influence of these southern-sourced waters would result in warmer temperatures at the location of Site 1236. Parallel to the constriction of the Indonesian Gateway at ~3.5 Ma (Karas et al., 2009), SOIW became more dominant at subtropical West Pacific subsurface level and resulted in the gradual cooling of these waters (Karas et al., 2011; McClymont et al., 2016). In a similar way, the northward expansion of SOIW in the East Pacific could have contributed to the gradual cooling observed in $TT_{G. tumida}$ at our site after ~3.5 Ma. Likewise, decreased SOIW influence between ~3.8 and 3.5 Ma might explain the warming $TT_{G. tumida}$ trend at Site 1236. Although we cannot rule out a contribution of this process to the pattern observed by us, a second process must have acted upon $TT_{G. tumida}$, as no warming trend was observed between 3.8 and 3.5 Ma by deeper dwelling *G. inflata* (Figure 6). As this pattern is only observed by *G. tumida*, we argue that the largest change in subsurface processes must have occurred between the habitat depth of *G. tumida* and *G. inflata*.

At ~21°S, the tongue of SOIW is about 2–3 °C colder than modern NPIW to the north of the equator (Locarnini et al., 2013). Replacing the influence of SOIW with slightly warmer NPIW would thus result in a $TT_{G. tumida}$ increase at Site 1236 similar to the pattern observed by us (Figure 6). The rivaling influence of NPIW and SOIW in the equatorial East Pacific was previously demonstrated for the last two glacial-interglacial cycles (Rippert et al., 2017). Reconstructed $\delta^{13}C$ records on the subthermocline species *Globorotaloides hexagonus* indicate the dominant presence of NPIW during peak glacial, and SOIW during interglacial periods (Rippert et al., 2017). The ACD of *G. hexagonus* (340–430 m; Rippert et al., 2016) is close to the ACD of *G. inflata* (Groeneveld & Chiessi, 2011). Thus, we would expect to see this pattern in our *G. inflata* record, parallel to the *G. tumida* warming signal. If slightly warmer NPIW would have penetrated from the north, we would also expect to observe the warming signal in both northern sites (1239/1241) and not only at our South Pacific Site.

As we discussed above, the westward directed equatorial trade winds cause upwelling along the equator. Their motion results in a thermocline “bulge” that deepens toward the north and the south (Figures 7 and 8), resulting in elevated $TT_{G. tumida}$ at modern Site 1236, when compared to Sites 1239 and 1241 (Figures 7 and 8). While previous studies primarily focused on the evolution of the zonal gradient between the East and West Pacific (e.g., Wara et al., 2005; Zhang et al., 2014), we present a new meridional perspective of thermocline depth and temperatures, independent from the permanent El Niño discussion. As tropical precipitation is intimately coupled to the location of the ITCZ, several proxy records highlight a glacial-interglacial

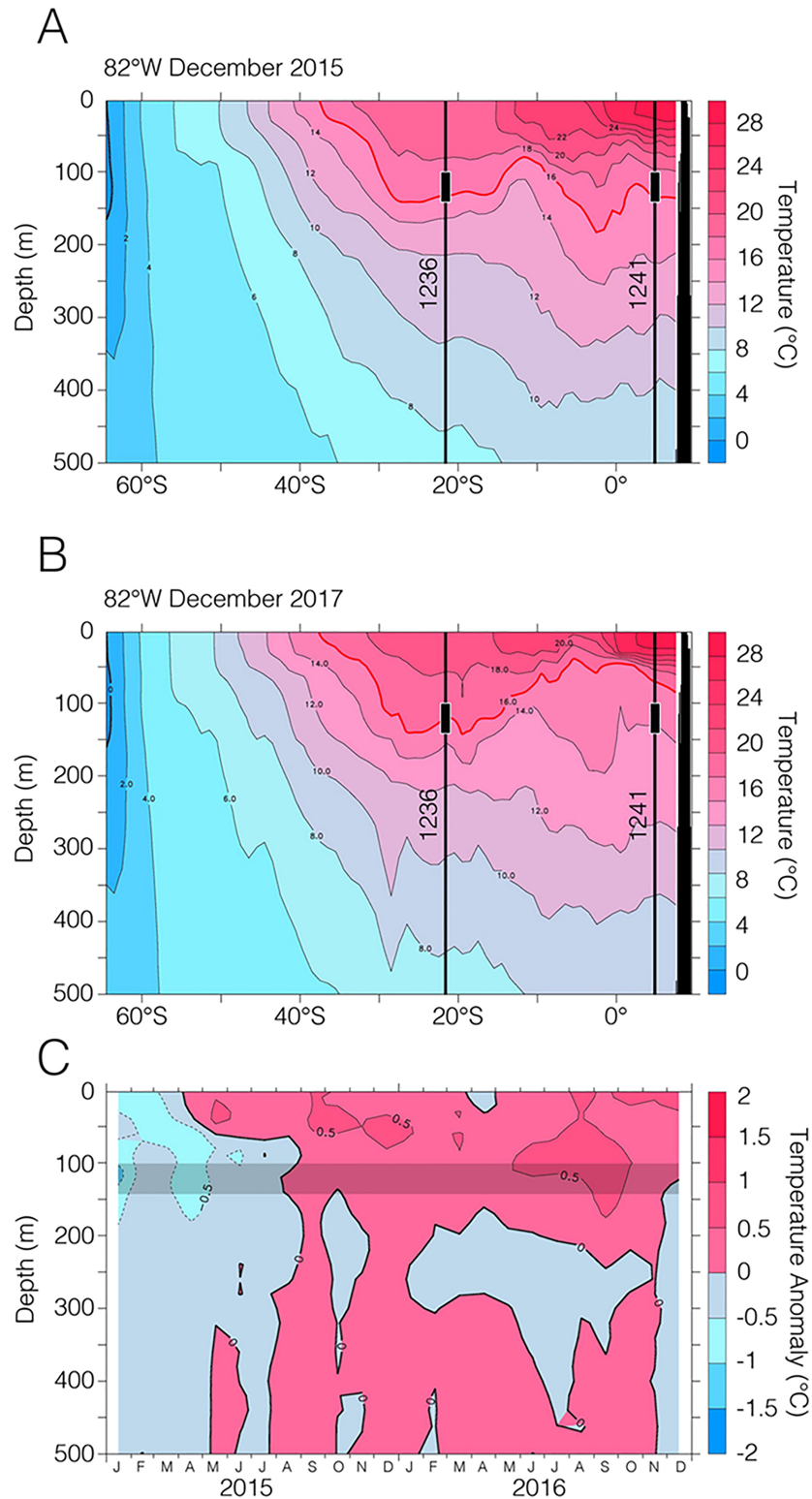


Figure 8. Temperature section along the black line indicated in Figure 1b. (a) El Niño year of 2015 versus (b) the reference year of 2017. Red lines indicate the 16 °C isotherm, which is the most dominant isotherm of the BOPZ during an El Niño event. Comparing 2015 and 2017, the development of the thermocline bulge discussed here becomes apparent. Despite its southern location, the BOPZ at 1236 is also experiencing a considerable warming during an El Niño event. Black lines indicate the water masses above Sites 1236/1241. Black boxes mark the average habitat depth of *G. tumida*. (c) Time series of temperature anomalies (versus monthly average) during the 2015/2016 El Niño event at the location of Site 1236. The grey bar indicates the average habitat depth of *G. tumida* (Argo Program, 2019).

displacement of rainfall patterns, hence the ITCZ, toward the warmer hemisphere (Broccoli et al., 2006; Clark et al., 2012; Escobar et al., 2012; McGee et al., 2014; Wang et al., 2004; Wang & Rong, 2007). While the movement of the ITCZ and the SPH is by now a well-established mechanism (Broccoli et al., 2006; Chiang et al., 2014; Schneider et al., 2017), there is no information on the Pliocene evolution of the oceanic (upwelling) response to latitudinal changes in the ITCZ/SPH wind systems.

The BOPZ temperature ($TT_{G. tumida}$) increase observed between 3.8 and 3.5 Ma indicates the northward movement of the SPH and the ITCZ, and thus of the trade winds. This process places the BOPZ of Sites 1239 and 1241 in the direct vicinity of the thermocline, while the TCD increases toward the south. As seen in Figure 2c, the ACD of *G. tumida* is right at the depth of the modern thermocline. The north-eastward movement of the SPH (and the northerly ITCZ) places this depth under the influence of warmer waters above the thermocline. At the same time $subSST_{T. sacculifer}$ also warm (Figure 4). The observed thermocline deepening (as indicated by the increasing $TT_{G. tumida}$ temperatures) likely also affected the calcification depth of *T. sacculifer* (subSST), triggering the observed increase in temperatures. Following this first formation of the temperature bulge, the subsequent cooling observed in our $TT_{G. tumida}$ record suggests a gradual shoaling of East Pacific TCD into the Pleistocene. After 3 Ma, Steph et al. (2006) observed a significant temperature increase at the BOPZ ($TT_{G. tumida}$). This increase can result from a relaxation of the meridional East Pacific temperature gradient, causing a decreased gradient of $TT_{G. tumida}$ at the northern sites and South Pacific Site 1236 (Figure 7c). This relaxation argues for the southward movement of the ITCZ/SPH system, slowly establishing the modern temperature gradient between Sites 1236 and 1241. Both northern sites experienced a phase of thermocline deepening between ~3.0 and 2.4 Ma (Steph et al., 2010). Following our hypothesis, this phase points to the southward movement of the bulge and its associated TCD (Figure 7c).

Our records show that a gradual shoaling of the TCD affected the deeper waters (*G. inflata*) between 4 and 2.5 Ma. Following this time period, no significant trend in their respective temperatures is observed. Hence, we assume that thereafter, this water depth permanently remained below the depth of the constantly shoaling East Pacific thermocline. However, indicated by our *G. tumida* record (Figure 4) the East Pacific thermocline continued to shoal throughout the entire time period from 3.5 to ~0.13 Ma.

The very long interval over which the shoaling of the East Pacific TCD occurred, points toward a slow and steady driving force behind these processes. The long-term formation of the northern hemisphere ice cap (Fedorov et al., 2006) and/or tectonic processes (Karas et al., 2009; Steph et al., 2006, 2010) are likely candidates to have caused the perturbation in the Pliocene and Pleistocene eastern Pacific water column.

Two ocean gateways, crucial to global oceanic circulation, closed or narrowed parallel to the changes observed in the East Pacific water column. A critical threshold in the closure of the CAS was reached between 4.7 and 4.2 Ma in the East Pacific (Haug et al., 2001). The CAS closure had a significant impact on circulation patterns of the Atlantic and the Pacific and is considered to be a likely candidate for the amplification of the Northern Hemisphere glaciation (Haug & Tiedemann, 1998; Hay, 1996).

Throughout the tropical Pacific, the CAS closure was accompanied by cooling equatorial Pacific SSTs, while the magnitude and evolution of the west-east gradient and the permanent El Niño-like conditions are still a matter of an ongoing debate (Bonham et al., 2009; Haug & Tiedemann, 1998; Ravelo et al., 2004; Steph et al., 2006; Wara et al., 2005; Watanabe et al., 2011; Zhang et al., 2014). In addition to these processes, thermocline temperature reconstructions indicate a progressive shoaling of the East Pacific thermocline during the Plio-Pleistocene (Steph et al., 2010; Zhang et al., 2012; this study). However, the timing of changes in East Pacific indicates that different or additional processes affected the meridional development of TCD. Following the closure of the CAS, a strengthening of the global thermohaline circulation resulted in the intensification of the Atlantic Meridional Overturning Circulation since ~4.6 Ma (Haug & Tiedemann, 1998; Karas et al., 2017), transporting moisture and heat to the Northern Hemisphere. In turn, the ITCZ/SPH system moves toward the warmer hemisphere (Broccoli et al., 2006) and displaces the position of the Walker Circulation and the trade winds to the north. The northward displacement of the equatorial wind systems induced a similar shift in the equatorial thermocline bulge and placed the BOPZ of Site 1236 (this study) in warmer waters compared to northerly Site 1241 (Steph et al., 2006; Figure 7b). During the time interval in question (~3.8–3.5 Ma) however, North Atlantic $subSST_{T. sacculifer}$ declined, while southern tropical Atlantic temperatures increased (Karas et al., 2017). This pattern most likely resulted in a weakened Atlantic Meridional

Overturing Circulation and thus a reduced heat transport toward the Northern Hemisphere, hence hampering the northward migration of the ITCZ/SPH system. While there is no modern analogue to a comparable overturning circulation in the Pacific (PMOC), data and modeling evidence show that a distinct PMOC existed in the Pliocene Pacific, transporting heat from the Southern Hemisphere to the north (Burls et al., 2017). These reconstructions show a rapid PMOC strengthening between ~4 and 3 Ma (Burls et al., 2017) that resulted in pronounced warming of the Northern Pacific and presumably accounted for the northward displacement of the ITCZ/SPH. As a reaction to the gradual intensification of the NHG after ~2.4 Ma (Raymo, 1994), $TT_{G. tumida}$ at our core location started to continuously cool all the way into the Pleistocene (Figure 4). The Northern Hemisphere cooling slowly forced a gradual shift in the location of the ITCZ/SPH system toward the south. This shift moved the trade winds and upwelling systems closer to our site; thus, it gradually diminished the temperature gradient between 1236 and 1241 (Figure 7c). Our interpretation of the north-south movement of the ITCZ/SPH system and the thermocline bulge does not rely on the presence or absence of Pliocene El Niño-like conditions or the noted presence or absence of a west-east SST gradient (Karas et al., 2009; Steph et al., 2006, 2010; Wara et al., 2005; Watanabe et al., 2011; Zhang et al., 2012; Zhang et al., 2014).

While the long-term shoaling of the East Pacific TCD and the development of the zonal Pacific SST gradient was a result of the closure/constriction of oceanic gateways (CAS and IG), we argue that the meridional evolution of BOPZ temperatures ($TT_{G. tumida}$) in the East Pacific was mostly driven by the north-south movement of the ITCZ/SPH system that was in turn forced by the intensification of the Gulf Stream, the PMOC, and later on by the increased NHG.

The offset of our youngest data points at ~135 ka to modern East Pacific temperatures (Figure 4b; Locarnini et al., 2013) likely reflects the Pleistocene evolution of the East Pacific cold tongue (Liu et al., 2019).

5. Summary and Conclusions

Our reconstructions of Pliocene and Pleistocene changes in East Pacific subsurface and thermocline temperatures shed new light on the evolution of the Pacific thermocline depth. Based on Mg/Ca-derived records, the subSST_{T. sacculifer} evolution at Site 1236 shows no distinctive trend and maintains a more or less constant offset to the tropical West Pacific (Figure 6; Wara et al., 2005). Using Mg/Ca temperatures from deeper dwelling *G. tumida*, Steph et al. (2006) were able to show that the shoaling of East Pacific TCD affected the BOPZ ($TT_{G. tumida}$) already at ~4.8 Ma.

While the zonal gradient in thermocline evolution is widely examined, our data add a so far unconsidered meridional component to these reconstructions. We are able to show that the East Pacific water column was not homogenous between ~4 and 2.7 Ma. Rather it was marked by a pronounced meridional difference between the doldrums sites to the north and the South Pacific (Figure 7). While the $TT_{G. tumida}$ at the doldrums reached modern-like values during this time period (Steph et al., 2006), our data show a pronounced increase in $TT_{G. tumida}$ between 3.8 and 3.5 Ma that was followed by a gradual decline toward the Pleistocene. The $TT_{G. tumida}$ gradient—highlighted in Figures 6 and 7—points to a three-dimensional thermocline pattern that began to form at ~3.8 Ma. The first component of this pattern is the known zonal evolution throughout the Plio-Pleistocene (Groeneveld et al., 2006; Steph et al., 2006; Steph et al., 2010; Wara et al., 2005; Y. G. Zhang et al., 2014). The second component is the northward movement of the ITCZ/SPH system and thus the equatorial temperature bulge that slopes toward the north and the south (Figure 7). Compared to ODP Site 1241 (Steph et al., 2006) we propose that coupled to the position of the ITCZ/SPH and their wind systems, the latitudinal dimension of this bulge might have been more variable through time. Hence, it might be more prone to local or short-termed changes caused by a reorganization of global temperatures.

According to the IPCC, the ongoing global warming may favor more El Niño-like conditions over the next centuries via the weakening of the equatorial Walker circulation (Vecchi & Soden, 2007). This weakening will result in a deepening of the East Pacific thermocline and diminish the eastward transport of subsurface waters from the West to the East Pacific. However, this transport is crucial for the supply of micronutrients from volcanic influenced regions in the west toward the high-chlorophyll low-nutrient area in the east (Behrens et al., 2018). Furthermore, a warming globe might also cause significant changes in the position of the ITCZ/SPH (Schneider et al., 2017). Our study shows that this process could affect equatorial regions

more intensively due to the potential temperature-driven movement of the ITCZ/SPH and thus, the equatorial thermocline bulge. To achieve a more detailed picture of the evolution of the East Pacific ITCZ, the SPH, and the associated development and meridional movement of the thermocline bulge during the Warm Pliocene, we need a better meridional resolution of sediment records, covering the modern position of the bulge (Figure 8b).

Acknowledgments

This work was funded by the Federal Ministry of Education and Research (BMBF; Germany) project 03G0213A – SOPATRA and DFG SPP-1158 project RO5057/1-2. We thank the crew and shipboard party of R/V *JOIDES Resolution* Leg 202, A. Mackensen, S. Steph for the data, and S. Fessler, R. Fröhlking-Teichert, N. Gehre, G. Meyer, L. Schönborn, S. Schumacher, M. Seebeck, and S. Wiebe for the technical support. Thanks to P. Rafter for providing the *Life Aquatic* ODV palette. Data are accessible at <https://doi.pangaea.de/10.1594/PANGAEA.896166>.

References

- Anand, P., Elderfield, H., & Conte, M. H. (2003). Calibration of Mg/Ca thermometry in planktonic foraminifera from a sediment trap time series. *Paleoceanography*, *18*(2), 1050. <https://doi.org/10.1029/2002PA000846>
- Argo Program. (2019). Argo temperature data.
- Ayón, P., Criales-Hernandez, M. I., Schwamborn, R., & Hirche, H.-J. (2008). Zooplankton research off Peru: A review. *Progress in Oceanography*, *79*(2-4), 238–255. <https://doi.org/10.1016/j.pocean.2008.10.020>
- Behrens, M. K., Pahnke, K., Schnetger, B., & Brumsack, H.-J. (2018). Sources and processes affecting the distribution of dissolved Nd isotopes and concentrations in the West Pacific. *Geochimica et Cosmochimica Acta*, *222*, 508–534. <https://doi.org/10.1016/j.gca.2017.11.008>
- Bonham, S. G., Haywood, A., Lunt, D. J., Collins, M., & Salzmann, U. (2009). El Niño–Southern Oscillation, Pliocene climate and equifinality. *Philosophical Transactions of the Royal Society*, *367*(1886), 127–156. <https://doi.org/10.1098/rsta.2008.0212>
- Broccoli, A. J., Dahl, K. A., & Stouffer, R. J. (2006). Response of the ITCZ to Northern Hemisphere cooling. *Geophysical Research Letters*, *33*, L01702. <https://doi.org/10.1029/2005GL024546>
- Burls, N. J., Fedorov, A. V., Sigman, D. M., Jaccard, S. L., Tiedemann, R., & Haug, G. H. (2017). Active Pacific meridional overturning circulation (PMOC) during the warm Pliocene. *Science Advances*, *3*, e1700156. <https://doi.org/10.1126/sciadv.1700156>
- Cai, W., Borlace, S., Lengaigne, M., van Rensch, P., Collins, M., Vecchi, G. A., et al. (2014). Increasing frequency of extreme El Niño events due to greenhouse warming. *Nature Climate Change*, *4*(2), 111–116. <https://doi.org/10.1038/nclimate2100>
- Cane, M. A. (2005). The evolution of El Niño, past and future. *Earth and Planetary Science Letters*, *230*(3-4), 227–240. <https://doi.org/10.1016/j.epsl.2004.12.003>
- Cane, M. A., & Molnar, P. (2001). Closing of the Indonesian seaway as a precursor to east African aridification around 3–4 million years ago. *Nature*, *411*(6834), 157–162. <https://doi.org/10.1038/35075500>
- Chiang, J. C. H., Lee, S.-Y., Putnam, A. E., & Wang, X. (2014). South Pacific Split Jet, ITCZ shifts, and atmospheric North–South linkages during abrupt climate changes of the last glacial period. *Earth and Planetary Science Letters*, *406*, 233–246. <https://doi.org/10.1016/j.epsl.2014.09.012>
- Clark, P. U., Shakun, J. D., Baker, P. A., Bartlein, P. J., Brewer, S., Brook, E., et al. (2012). Global climate evolution during the last deglaciation. *PNAS*, *109*(19), E1134–E1142. <https://doi.org/10.1073/pnas.1116619109>
- Curry, W. B., Thunell, R. C., & Honjo, S. (1983). Seasonal changes in the isotopic composition of planktonic foraminifera collected in Panama Basin sediment traps. *Earth and Planetary Science Letters*, *64*(1), 33–43. [https://doi.org/10.1016/0012-821X\(83\)90050-X](https://doi.org/10.1016/0012-821X(83)90050-X)
- Dekens, P. S., Ravelo, A. C., & McCarthy, M. D. (2007). Warm upwelling regions in the Pliocene warm period. *Paleoceanography*, *22*, PA3211. <https://doi.org/10.1029/2006PA001394>
- Dowsett, H. J., & Robinson, M. M. (2009). Mid-Pliocene equatorial Pacific sea surface temperature reconstruction: A multi-proxy perspective. *Philosophical Transactions of the Royal Society*, *367*(1886), 109–125. <https://doi.org/10.1098/rsta.2008.0206>
- Duplessy, J.-C., Bé, A. W. H., & Blanc, P. L. (1981). Oxygen and carbon isotopic composition and biogeographic distribution of planktonic foraminifera in the Indian Ocean. *Palaeogeography, Palaeoclimatology, Palaeoecology*, *33*(1-3), 9–46. [https://doi.org/10.1016/0031-0182\(81\)90031-6](https://doi.org/10.1016/0031-0182(81)90031-6)
- Escobar, J., Hodell, D. A., Brenner, M., Curtis, J. H., Gilli, A., Mueller, A. D., et al. (2012). A ~43-ka record of paleoenvironmental change in the Central American lowlands inferred from stable isotopes of lacustrine ostracods. *Quaternary Science Reviews*, *37*, 92–104. <https://doi.org/10.1016/j.quascirev.2012.01.020>
- Etourneau, J., Schneider, R., Blanz, T., & Martinez, P. (2010). Intensification of the Walker and Hadley atmospheric circulations during the Pliocene–Pleistocene climate transition. *Earth and Planetary Science Letters*, *297*(1-2), 103–110. <https://doi.org/10.1016/j.epsl.2010.06.010>
- Fairbanks, R. G., Sverdrup, M., Free, R., Wiebe, P. H., & Bé, A. W. H. (1982). Vertical distribution and isotopic fractionation of living planktonic foraminifera from the Panama Basin. *Nature*, *298*(5877), 841–844. <https://doi.org/10.1038/298841a0>
- Fairbanks, R. G., & Wiebe, P. H. (1980). Foraminifera and chlorophyll maximum: Vertical distribution, seasonal succession, and paleoceanographic significance. *Science*, *209*(4464), 1524–1526. <https://doi.org/10.1126/science.209.4464.1524>
- Fairbanks, R. G., Wiebe, P. H., & Be, A. W. (1980). Vertical distribution and isotopic composition of living planktonic foraminifera in the western North Atlantic. *Science*, *207*(4426), 61–63. <https://doi.org/10.1126/science.207.4426.61>
- Fedorov, A. V., Dekens, P. S., McCarthy, M. D., Ravelo, A. C., deMenocal, P. B., Barreiro, M., et al. (2006). The Pliocene paradox (mechanisms for a permanent El Niño). *Science*, *312*(5779), 1485–1489. <https://doi.org/10.1126/science.1122666>
- Fiedler, P. C., & Talley, L. D. (2006). Hydrography of the eastern tropical Pacific: A review. *Progress in Oceanography*, *69*(2-4), 143–180. <https://doi.org/10.1016/j.pocean.2006.03.008>
- Filippelli, G. M., & Flores, J.-A. (2009). From the warm Pliocene to the cold Pleistocene: A tale of two oceans. *Geology*, *37*(10), 959–960. <https://doi.org/10.1130/focus102009.1>
- Greaves, M., Caillon, N., Rebaubier, H., Bartoli, G., Cacho, I., Clarke, L., et al. (2008). Interlaboratory comparison study of calibration standards for foraminiferal Mg/Ca thermometry. *Geochemistry, Geophysics, Geosystems*, *9*, Q08010. <https://doi.org/10.1029/2008GC001974>
- Groeneveld, J., & Chiessi, C. M. (2011). Mg/Ca of *Globorotalia inflata* as a recorder of permanent thermocline temperatures in the South Atlantic. *Paleoceanography*, *26*, PA2203. <https://doi.org/10.1029/2010PA001940>
- Groeneveld, J., Steph, S., Tiedemann, R., Garbe-Schönberg, D., Nürnberg, D., & Sturm, A. (2006). Pliocene development of east-Pacific hydrology as revealed by Mg/Ca analyses on the planktic foraminifer *Globigerinoides sacculifer*. In *ODP Scientific Results, Leg 202* (Chap. 209). College Station, TX.
- Haug, G. H., & Tiedemann, R. (1998). Effect of the formation of the Isthmus of Panama on Atlantic Ocean thermohaline circulation. *Nature*, *393*(6686), 673–676. <https://doi.org/10.1038/31447>

- Haug, G. H., Tiedemann, R., Zahn, R., & Ravelo, A. C. (2001). Role of Panama uplift on oceanic freshwater balance. *Geology*, *29*(3), 207–210. [https://doi.org/10.1130/0091-7613\(2001\)029<0207:ROPULL>2.0.CO;2](https://doi.org/10.1130/0091-7613(2001)029<0207:ROPULL>2.0.CO;2)
- Hay, W. W. (1996). Tectonics and climate. *Geologische Rundschau*, *85*(3), 409–437. <https://doi.org/10.1007/BF02369000>
- Haywood, A., Dowsett, H. J., Valdes, P. J., Lunt, D. J., Francis, J. E., & Sellwood, B. W. (2009). Pliocene climate, processes and problems. *Philosophical Transactions of the Royal Society*, *367*(1886), 3–17. <https://doi.org/10.1098/rsta.2008.0205>
- Hemleben, C., Spindler, C., & Anderson, O. R. (1988). *Modern planktonic foraminifera*. New York: Springer.
- Ibaraki, M. (1997). Closing of the Central American Seaway and Neogene coastal upwelling along the Pacific coast of South America. *Tectonophysics*, *281*(1–2), 99–104. [https://doi.org/10.1016/S0040-1951\(97\)00161-3](https://doi.org/10.1016/S0040-1951(97)00161-3)
- Jentzen, M. F., Nummelin, A., Nielsen, S. B., Sadatzki, H., Sessford, E., Risebrobakken, B., et al. (2018). A spatiotemporal reconstruction of sea-surface temperatures in the North Atlantic during Dansgaard–Oeschger events 5–8. *Climate of the Past*, *14*(6), 901–922. <https://doi.org/10.5194/cp-14-901-2018>
- Karas, C., Nürnberg, D., Bahr, A., Groeneveld, J., Herrle, J. O., Tiedemann, R., & de Menocal, P. B. (2017). Pliocene oceanic seaways and global climate. *Scientific Reports*, *7*, 39842. <https://doi.org/10.1038/srep39842>
- Karas, C., Nürnberg, D., Gupta, A. K., Tiedemann, R., Mohan, K., & Bickert, T. (2009). Mid-Pliocene climate change amplified by a switch in Indonesian subsurface throughflow. *Nature Geoscience*, *2*(6), 434–438. <https://doi.org/10.1038/ngeo520>
- Karas, C., Nürnberg, D., Tiedemann, R., & Garbe-Schönberg, D. (2011). Pliocene climate change of the Southwest Pacific and the impact of ocean gateways. *Earth and Planetary Science Letters*, *301*(1–2), 117–124. <https://doi.org/10.1016/j.epsl.2010.10.028>
- Karstensen, J., & Ulloa, O. (2008). The Peru–Chile Current System. In J. H. Steele, S. A. Thorpe, & K. K. Turekian (Eds.), *Encyclopedia of Ocean Sciences* (Vol. 2e, pp. 385–392). London: Academic Press.
- Keigwin, L. D. (1982). Isotopic paleoceanography of the Caribbean and East Pacific: Role of Panama uplift in late Neogene time. *Science*, *217*(4557), 350–353. <https://doi.org/10.1126/science.217.4557.350>
- Kessler, W. S. (2006). The circulation of the eastern tropical Pacific: A review. *Progress in Oceanography*, *69*(2–4), 181–217. <https://doi.org/10.1016/j.pocean.2006.03.009>
- Latif, M., Semenov, V. A., & Park, W. (2015). Super El Niños in response to global warming in a climate model. *Climatic Change*, *132*(4), 489–500. <https://doi.org/10.1007/s10584-015-1439-6>
- Lenton, T. M., Held, H., Kriegler, E., Hall, J. W., Lucht, W., Rahmstorf, S., & Schnellhuber, H. J. (2008). Tipping elements in the Earth's climate system. *PNAS*, *105*(6), 1786–1793. <https://doi.org/10.1073/pnas.0705414105>
- Letelier, J., Pizarro, O., & Nuñez, S. (2009). Seasonal variability of coastal upwelling and the upwelling front off central Chile. *Journal of Geophysical Research*, *114*, C12009. <https://doi.org/10.1029/2008JC005171>
- Lisiecki, L. E., & Raymo, M. E. (2005). A Pliocene–Pleistocene stack of 57 globally distributed benthic $\delta^{18}\text{O}$ records. *Paleoceanography*, *20*, PA1003. <https://doi.org/10.1029/2004PA001071>
- Lisiecki, L. E., & Raymo, M. E. (2007). Plio–Pleistocene climate evolution: Trends and transitions in glacial cycle dynamics. *Quaternary Science Reviews*, *26*(1–2), 56–69. <https://doi.org/10.1016/j.quascirev.2006.09.005>
- Liu, J., Tian, J., Liu, Z., Herbert, T. D., Fedorov, A. V., & Leyle, M. (2019). Eastern equatorial Pacific cold tongue evolution since the late Miocene linked to extratropical climate. *Science Advances*, *5*, eaau6060. <https://doi.org/10.1126/sciadv.aau6060>
- Locarnini, R. A., Mishonov, A. V., Antonov, J. I., Boyer, T. P., Garcia, H. E., Baranova, O. K., et al. (2013). Temperature. In S. Levitus & A. V. Mishonov (Eds.), *World Ocean Atlas 2013* (Vol. 1, pp. 1–27). Silver Spring, MD: NOAA.
- Lohmann, G. P. (1995). A model for variation in the chemistry of planktonic foraminifera due to secondary calcification and selective dissolution. *Paleoceanography*, *10*(3), 445–457. <https://doi.org/10.1029/95PA00059>
- Lunt, D. J., Haywood, A., Foster, G. L., & Stone, E. J. (2009). The Arctic cryosphere in the Mid-Pliocene and the future. *Philosophical Transactions of the Royal Society*, *367*(1886), 49–67. <https://doi.org/10.1098/rsta.2008.0218>
- Lunt, D. J., Valdes, P. J., Haywood, A., & Rutt, I. C. (2007). Closure of the Panama Seaway during the Pliocene: Implications for climate and Northern Hemisphere glaciation. *Climate Dynamics*, *30*(1), 1–18. <https://doi.org/10.1007/s00382-007-0265-6>
- Lynch-Stieglitz, J., Polissar, P. J., Jacobel, A. W., Hovan, S. A., Pockalny, R. A., Lyle, M., et al. (2015). Glacial–interglacial changes in central tropical Pacific surface seawater property gradients. *Paleoceanography*, *30*, 423–438. <https://doi.org/10.1002/2014PA002746>
- McClymont, E. L., Elmore, A. C., Kender, S., Leng, M. J., Greaves, M., & Elderfield, H. (2016). Pliocene–Pleistocene evolution of sea surface and intermediate water temperatures from the southwest Pacific. *Paleoceanography*, *31*, 895–913. <https://doi.org/10.1002/2016PA002954>
- McGee, D., Donohoe, A., Marshall, J., & Ferreira, D. (2014). Changes in ITCZ location and cross-equatorial heat transport at the Last Glacial Maximum, Heinrich Stadial 1, and the mid-Holocene. *Earth and Planetary Science Letters*, *390*, 69–79. <https://doi.org/10.1016/j.epsl.2013.12.043>
- McPhaden, M. J., Zebiak, S. E., & Glantz, M. H. (2006). ENSO as an integrating concept in Earth science. *Science*, *314*(5806), 1740–1745. <https://doi.org/10.1126/science.1132588>
- Meschede, M., & Barckhausen, U. (2000). Plate tectonic evolution of the Cocos–Nazca spreading center. *Proceeding of the Ocean Drilling Program, Scientific Results*, *170*, 1–10. <https://doi.org/10.2973/odp.proc.sr.170.009>
- Miller, K. G., Raymo, M. E., Browning, J. V., Rosenthal, Y., & Wright, J. D. (2019). Peak sea level during the warm Pliocene: Errors, limitations, and constraints. *PAGES Magazine*, *27*(1), 1–2.
- Mix, A. C., Tiedemann, R., & Blum, P. (2003a). Leg 202 summary. *Proceedings of the Ocean Drilling Program, Initial Reports*, *202*, 1–145.
- Mix, A. C., Tiedemann, R., & Blum, P. (2003b). Site 1236. *Proceedings of the Ocean Drilling Program, Initial Reports*, *202*, 1–74.
- Pagani, M., Liu, Z., LaRivière, J., & Ravelo, A. C. (2010). High Earth–system climate sensitivity determined from Pliocene carbon dioxide concentrations. *Nature Geoscience*, *3*(1), 27–30. <https://doi.org/10.1038/ngeo724>
- Paillard, D., Labeyrie, L., & Yiou, P. (1996). Macintosh program performs time-series analysis. *Eos, Transactions of the American Geophysical Union*, *77*(39), 379. <https://doi.org/10.1029/96EO00259>
- Pena, L. D., Goldstein, S. L., Hemming, S. R., Jones, K. M., Calvo, E., Pelejero, C., & Cacho, I. (2013). Rapid changes in meridional advection of Southern Ocean intermediate waters to the tropical Pacific during the last 30 kyr. *Earth and Planetary Science Letters*, *368*, 20–32. <https://doi.org/10.1016/j.epsl.2013.02.028>
- Philander, S. G., & Fedorov, A. V. (2003a). Is El Niño sporadic or cyclic? *Annual Review of Earth and Planetary Sciences*, *31*(1), 579–594. <https://doi.org/10.1146/annurev.earth.31.100901.141255>
- Philander, S. G., & Fedorov, A. V. (2003b). Role of tropics in changing the response to Milankovich forcing some three million years ago. *Paleoceanography*, *18*(2), 1045. <https://doi.org/10.1029/2002PA000837>
- Raddatz, J., Nürnberg, D., Tiedemann, R., & Rippert, N. (2017). Southeastern marginal West Pacific Warm Pool sea-surface and thermocline dynamics during the Pleistocene (2.5–0.5 Ma). *Palaeogeography, Palaeoclimatology, Palaeoecology*, *471*, 144–156. <https://doi.org/10.1016/j.palaeo.2017.01.024>

- Ravelo, A. C., Andreasen, D. H., Lyle, M., Olivarez Lyle, A., & Wara, M. W. (2004). Regional climate shifts caused by gradual global cooling in the Pliocene epoch. *Nature*, *429*(6989), 263–267. <https://doi.org/10.1038/nature02567>
- Ravelo, A. C., & Fairbanks, R. G. (1992). Oxygen isotopic composition of multiple species of planktonic foraminifera: Recorders of the modern photic zone temperature gradient. *Paleoceanography*, *7*(6), 815–831. <https://doi.org/10.1029/92PA02092>
- Ravelo, A. C., & Shackleton, N. J. (1995). Evidence for surface-water circulation changes at Site 851 in the eastern tropical Pacific Ocean. *Proceedings of the Ocean Drilling Program*, *138*, 503–514. <https://doi.org/10.2973/odp.proc.sr.138.126>
- Raymo, M. E. (1994). The initiation of Northern Hemisphere glaciation. *Annual Review of Earth and Planetary Sciences*, *22*(1), 353–383. <https://doi.org/10.1146/annurev.ea.22.050194.002033>
- Raymo, M. E., Grant, B., Horowitz, M., & Rau, G. H. (1996). Mid-Pliocene warmth: Stronger greenhouse and stronger conveyor. *Marine Micropaleontology*, *27*(1–4), 313–326. [https://doi.org/10.1016/0377-8398\(95\)00048-8](https://doi.org/10.1016/0377-8398(95)00048-8)
- Raymo, M. E., Lisiecki, L. E., & Nisancioglu, K. H. (2006). Plio-Pleistocene ice volume, Antarctic climate, and the global $d^{18}O$ record. *Science*, *313*(5786), 492–495. <https://doi.org/10.1126/science.1123296>
- Regenberg, M., Regenberg, A., Garbe-Schönberg, D., & Lea, D. W. (2014). Global dissolution effects on planktonic foraminiferal Mg/Ca ratios controlled by the calcite-saturation state of bottom waters. *Paleoceanography*, *29*, 127–142. <https://doi.org/10.1002/2013PA002492>
- Reiðig, S., Nürnberg, D., Bahr, A., Poggemann, D.-W., & Hoffmann, J. (2019). Southward displacement of the North Atlantic subtropical gyre circulation system during North Atlantic cold spells. *Paleoceanography and Paleoclimatology*, *34*, 866–885. <https://doi.org/10.1029/2018PA003376>
- Rippert, N., Max, L., Mackensen, A., Cacho, I., Povea, P., & Tiedemann, R. (2017). Alternating influence of northern versus southern-sourced water masses on the equatorial Pacific subthermocline during the past 240 ka. *Paleoceanography*, *32*, 1256–1274. <https://doi.org/10.1002/2017PA003133>
- Rippert, N., Nürnberg, D., Raddatz, J., Maier, E., Hathorne, E., Bijma, J., & Tiedemann, R. (2016). Constraining foraminiferal calcification depths in the western Pacific warm pool. *Marine Micropaleontology*, *128*, 14–27. <https://doi.org/10.1016/j.marmicro.2016.08.004>
- Schlitzer, R. (2019). Ocean Data View (version 4.7.2.). [owa.awi.de](http://www.awi.de)
- Schmidt, M. W., & Lynch-Stieglitz, J. (2011). Florida Straits deglacial temperature and salinity change: Implications for tropical hydrologic cycle variability during the Younger Dryas. *Paleoceanography*, *26*, PA4205. <https://doi.org/10.1029/2011PA002157>
- Schneider, W., Donoso, D., Garcés-Vargas, J., & Escribano, R. (2017). Water-column cooling and sea surface salinity increase in the upwelling region off central-south Chile driven by a poleward displacement of the South Pacific High. *Progress in Oceanography*, *151*, 38–48. <https://doi.org/10.1016/j.pocean.2016.11.004>
- Seki, O., Foster, G. L., Schmidt, D. N., Mackensen, A., Kawamura, K., & Pancost, R. D. (2010). Alkenone and boron-based Pliocene pCO_2 records. *Earth and Planetary Science Letters*, *292*(1–2), 201–211. <https://doi.org/10.1016/j.epsl.2010.01.037>
- Silva, N., Rojas, N., & Fedele, A. (2009). Water masses in the Humboldt Current System: Properties, distribution, and the nitrate deficit as a chemical water mass tracer for Equatorial Subsurface Water off Chile. *Deep Sea Research, Part II*, *56*(16), 1004–1020. <https://doi.org/10.1016/j.dsr2.2008.12.013>
- Spero, H. J., Mielke, K. M., Kalve, E. M., Lea, D. W., & Pak, D. K. (2003). Multispecies approach to reconstructing eastern equatorial Pacific thermocline hydrography during the past 360 kyr. *Paleoceanography*, *18*(1), 1022. <https://doi.org/10.1029/2002PA000814>
- Spezzaferri, S., Kucera, M., Pearson, P. N., Wade, B. S., Rappo, S., Poole, C. R., et al. (2015). Fossil and genetic evidence for the polyphyletic nature of the planktonic foraminifera “*Globigerinoides*,” and description of the new genus *Trilobatus*. *PLoS ONE*, *10*, e0128108. <https://doi.org/10.1371/journal.pone.0128108>
- Steph, S., Tiedemann, R., Groeneveld, J., Sturm, A., & Nürnberg, D. (2006). Pliocene changes in tropical East Pacific upper ocean stratification: Response to tropical gateways? *Proceeding of the Ocean Drilling Program, Scientific Results*, *202*, 1–51.
- Steph, S., Tiedemann, R., Prange, M., Groeneveld, J., Schulz, M., Timmermann, A., et al. (2010). Early Pliocene increase in thermohaline overturning: A precondition for the development of the modern equatorial Pacific cold tongue. *Paleoceanography*, *25*, PA2202. <https://doi.org/10.1029/2008PA001645>
- Strub, P. T., Mesías, J. M., Montecino, V., Rutllant, J., & Salinas, S. (1998). Coastal ocean circulation off western South America. In *The Sea, Coastal Oceans* (Vol. 11, pp. 273–313). New York: Wiley.
- Sun, D.-Z., Zhang, T., & Shin, S.-I. (2004). The effect of subtropical cooling on the amplitude of ENSO: A numerical study. *Journal of Climate*, *17*, 3786–3798. [https://doi.org/10.1175/1520-0442\(2004\)017<3786:TEOSCO>2.0.CO;2](https://doi.org/10.1175/1520-0442(2004)017<3786:TEOSCO>2.0.CO;2)
- Tiedemann, R., Mix, A. C., Richter, C., & Ruddiman, W. F. (2007). Astronomically calibrated timescales from 6 to 2.5 Ma and benthic isotope stratigraphies, Sites 1236, 1237, 1239, and 1241. *Proceeding of the Ocean Drilling Program, Scientific Results*, *202*, 1–69. <https://doi.org/10.2973/odp.proc.sr.202.210.2007>
- Timmermann, A., Oberhuber, J., Bacher, A., Esch, M., & Latif, M. (1999). Increased El Niño frequency in a climate model forced by future greenhouse warming. *Nature*, *398*(6729), 694–697. <https://doi.org/10.1038/19505>
- Vecchi, G. A., & Soden, B. J. (2007). Global warming and the weakening of the tropical circulation. *Journal of Climate*, *20*(17), 4316–4340. <https://doi.org/10.1175/JCLI4258.1>
- Wang, H., & Rong, F. (2007). The influence of Amazon rainfall on the Atlantic ITCZ through convectively coupled Kelvin waves. *Journal of Climate*, *20*(7), 1188–1201. <https://doi.org/10.1175/JCLI4061.1>
- Wang, X., Auler, A. S., Edwards, R. L., Cheng, H., Cristalli, P. S., Smart, P. L., et al. (2004). Wet periods in northeastern Brazil over the past 210 kyr linked to distant climate anomalies. *Nature*, *432*(7018), 740–743. <https://doi.org/10.1038/nature03067>
- Wara, M. W., Ravelo, A. C., & Delaney, M. L. (2005). Permanent El Niño-like conditions during the Pliocene warm period. *Science*, *309*(5735), 758–761. <https://doi.org/10.1126/science.1112596>
- Watanabe, T., Suzuki, A., Minobe, S., Kawashima, T., Kameo, K., Minoshima, K., et al. (2011). Permanent El Niño during the Pliocene warm period not supported by coral evidence. *Nature*, *471*(7337), 209–211. <https://doi.org/10.1038/nature09777>
- Watkins, J. M., Mix, A. C., & Wilson, J. (1998). Living planktic foraminifera in the central tropical Pacific Ocean: Articulating the equatorial “cold tongue” during La Niña, 1992. *Marine Micropaleontology*, *33*(3–4), 157–174. [https://doi.org/10.1016/S0377-8398\(97\)00036-4](https://doi.org/10.1016/S0377-8398(97)00036-4)
- Wong, A. P. S., & Johnson, G. C. (2003). South Pacific Eastern Subtropical Mode Water. *Journal of Physical Oceanography*, *33*(7), 1493–1509. [https://doi.org/10.1175/1520-0485\(2003\)033<1493:SPESMW>2.0.CO;2](https://doi.org/10.1175/1520-0485(2003)033<1493:SPESMW>2.0.CO;2)
- Zhang, X., Prange, M., Steph, S., Butzin, M., Krebs, U., Lunt, D. J., et al. (2012). Changes in equatorial Pacific thermocline depth in response to Panamanian seaway closure: Insights from a multi-model study. *Earth and Planetary Science Letters*, *317*–318, 76–84. <https://doi.org/10.1016/j.epsl.2011.11.028>
- Zhang, Y. G., Pagani, M., & Liu, Z. (2014). A 12-million-year temperature history of the tropical Pacific Ocean. *Science*, *344*(6179), 84–87. <https://doi.org/10.1126/science.1246172>